Evaporation residue cross section measurements for the ^{30}Si + ^{176}Yb reaction

K. Hajara, M. M. Musthafa ⓘ,* C. V. Midhun, Shaima Akbar, and P. T. M. Shan ⓘ
Department of Physics, Calicut University, Calicut University P.O, Malappuram, Kerala 673 635, India

N. Madhavan ⓘ, S. Nath ⓘ, J. Gehlot, Gonika, and Rohan Biswas ⓘ
Nuclear Physics Group, Inter University Accelerator Center, Aruna Asaf Ali Marg, New Delhi 110067, India

F. S. Shana
Department of Physics, Government Arts and Science College, Calicut, Kerala 673018, India

Amninder Kaur
Department of Physics, Panjab University, Chandigarh 160014, India

Prashant N. Patil
Department of Physics, KLE Technological University, B.V.B.C.E.T Campus, Hubballi, Karnataka 580031, India

Evaporation residue (ER) cross sections are measured for the reaction ^{30}Si + ^{176}Yb, which forms the compound nucleus ^{206}Po*, over the excitation energy range from 47.68 to 113.73 MeV. Dependence of noncompound nuclear reaction on entrance channel parameters such as charge product ($Z_1 Z_2$), mass asymmetry (α), deformation (β_2) of the target, and isospin asymmetry ($\Delta \frac{N}{Z}$) is explored. To analyze the experimental data the coupled-channels and the statistical model calculations are used. The measured ER cross sections are compared with the system, ^{12}C + ^{194}Pt forming the same compound nucleus and also with ^{28}Si + ^{176}Yb, forming ^{204}Po* in the neighborhood. Observed suppression in the evaporation residue cross sections at higher energies may be attributed to the presence of the noncompound nuclear process.

I. INTRODUCTION

Investigation of nuclear reaction dynamics near the Coulomb barrier is an active area of research even today. In the case of the heavy ion induced reaction, the quantum mechanical tunneling probability in the below barrier region is dramatically modified by coupling with various internal degrees of freedom leading to the enhanced reaction cross section, than predicted by the 1-dimensional barrier penetration model (1DBPM). This enhancement is accounted for, to a considerable extent, by exciting various internal degrees of freedom due to the coupling of rotational and vibrational excitations of the target and projectile in the presence of one another as well as the neutron transfer [1,2]. In the case of heavy ions with sufficient energy to overcome the Coulomb barrier and small impact parameter, there may be a complete fusion of the projectile with the target which results in the formation of a completely fused compound system. But the complete fusion of the projectile with the target is hindered due to the involvement of many noncompound phenomena such as quasifission, fast fission, and pre-equilibrium fission. These phenomena depend significantly on the entrance

channel properties like mass asymmetry [3–6], deformation [7–10], shell closure [11,12], and neutron excess of the colliding partners [13]. Signatures of these phenomena will be reflected in evaporation residue (ER) cross section [3,7], fission fragment angular distribution [14–16], and fission fragment mass distribution [3,17–19]. As the ER cross sections are the true signatures of compound nucleus formation, the reduction in the ER cross section is a clear indication of fusion suppression in the mass region $A \approx 200$ and beyond.

Berriman *et al.* measured the ER cross sections for reactions ^{12}C + ^{204}Pb, ^{19}F + ^{197}Au, and ^{30}Si + ^{186}W forming the compound nucleus ^{216}Ra* over the excitation energies 27 to 90 MeV. A significant inhibition of fusion is reported for ^{19}F and ^{30}Si induced reactions and it is attributed to the presence of quasifission [3]. Tripathi *et al.* measured the fission-fragment angular distributions for ^{19}F + ^{197}Au [20] and ^{24}Mg + ^{192}Os [21] reactions and the extracted results are consistent with the predictions of the statistical saddle-point model (SSPM) [22,23] negating the contribution of quasifission. Similarly, Tripathi *et al.* [24] measured the fission fragment angular distributions for the reactions ^{16}O + ^{188}Os and ^{28}Si + ^{176}Yb, which are consistent with the statistical model, and hence no contribution from noncompound nuclear fission is observed. However, the ER cross sections for the same system, ^{28}Si + ^{176}Yb, measured by Sudarshan *et al.*

*mmm@uoc.ac.in

[25] observed significant fusion suppression. Shamlath *et al.* [26] measured the fusion evaporation cross sections for the reactions ^{28,30}Si + ^{180}Hf and a significant contribution from the noncompound nuclear process is reported for both reactions. A similar contribution of noncompound fission is observed in the measurements of fission fragment mass distributions for the system, ^{30}Si + ^{180}Hf, by the same authors [27]. Mohanto *et al.* [28] measured ER-gated spin distribution for the ^{30}Si + ^{170}Er reaction forming CN ^{200}Pb*. The results were compared with those of two other systems, ^{16}O + ^{184}W and ^{19}F + ^{181}Ta [29], forming the same CN. The lowering of the spin is observed for the more symmetric system and is attributed to the presence of a noncompound nuclear reaction. Rajesh *et al.* [30] measured the ER cross sections for the reaction ^{48}Ti + ^{138}Ba and reported the presence of quasifission. Though considerable progress has been achieved on the dependence of fusion suppression on various entrance channel properties, the exact region from which the fusion probability starts to deviate from unity is to be identified. Hence, more experiments and systematic investigations of these results have to be carried out to understand the dependance of entrance channel parameters on fusion suppression and also to understand the exact region from which the fusion probability(P_{CN}) starts to deviate from unity.

In the present set of measurements, evaporation residue cross sections were measured for the system, ^{30}Si + ^{176}Yb, over the excitation energy range 47.68 to 113.73 MeV. The results are compared with those systems ^{12}C + ^{194}Pt [31], forming the same compound nucleus and also with that of the system, ^{28}Si + ^{176}Yb [25], forming a compound nucleus in the neighborhood.

II. EXPERIMENTAL DETAILS

The experiment was performed using the 15 UD Pelletron + SC–LINAC accelerator facility at IUAC, New Delhi. Pulsed beams of ^{30}Si, with a pulse separation of 250 ns, were bombarded on the isotopically enriched ^{176}Yb target of thickness $\approx$170 μg/cm^2 on a carbon backing of thickness $\approx$35 μg/cm^2. The target was positioned in such a way that the carbon backing was facing the beam. The cross section measurements were carried out at beam energies 203.02, 190.73, 180.45, 170.17, 159.85, 149.52, 144.45, 139.15, 136.16, 133.45, 131.94, 128.22, and 125.72 MeV. All these energies are the effective energies at the center (half-thickness) of the target, accounting for the energy loss of the incident beam at the entrance window foil of carbon with a thickness of 650 μg/cm^2, He gas of pressure 0.14 Torr between the window foil and target ($\sim$35 cm), 35 μg/cm^2 carbon backing facing the beam and 65 μg/cm^2 half-thickness of ^{176}Yb. In effect there is a loss of approximately 10 MeV as the incident Si beam reaches the center of the target. The ERs produced during the reaction were separated from the intense beam background using the hybrid recoil mass analyzer (HYRA) operated in gas-filled mode. HYRA is a dual-mode, dual-stage separator with its first stage capable of operating in gas-filled mode in normal kinematics [32,33]. Due to the velocity and charge state focusing, a gas-filled separator offers better transmission efficiency than vacuum-mode recoil separators. The frequent collision of

ERs with the gas molecules changes the energy and the charge state of the particles. In order to ensure better transmission efficiency, the optimization of the field values of dipole and quadrupole magnets and pressure of the gas used in HYRA have to be carried out. The field values used in HYRA are calculated using the simulation code developed in-house [34]. Helium gas at an optimized pressure of 0.15 mbar was used in the energy range of the present measurements. The field settings of HYRA magnets were optimized by scanning the field values within a range of $\pm$10% of the calculated values and the transmission through the separator was maximized at each energy.

Two silicon detectors were used inside the target chamber, placed at $\theta = \pm 26°$ to detect the elastically scattered beam particles and these detectors serve as monitor detectors for the absolute normalization of ER cross sections. A carbon foil of thickness 650 μg/cm^2 was used to separate the vacuum in the beam line and the gas-filled region in HYRA. The ERs produced during the reaction were transported to the focal plane of HYRA and detected there using a position-sensitive multiwire proportional counter (MWPC) [35] of active area 15 cm × 5 cm. The gas detector was operated with isobutane gas of about 2.5 mbar pressure. A large area mylar foil of thickness 0.5 micron was used to separate gas filled HYRA electromagnetic section and the focal plane detector. The MWPC counts were used for the measurement of ER cross sections after proper normalization. The detector was operated using isobutane gas at 2.5 mbar pressure and provided position, energy loss (ΔE) and timing signals. The position signals were processed through the constant fraction discriminator (CFD) and were fed to the time-to-digital converter (TDC) as a stop signal with an anode signal as the common start. Energy loss and energy signals from the MWPC cathode and monitors were fed to an analog to digital converter (ADC) after processing the preamplifier pulses through the shaping amplifiers. The logical OR of the timing signals from the monitor detectors and MWPC anode pulse acted as a master strobe for the data acquisition system. Data were collected and analyzed using IUAC data sorting software CANDLE [36].

III. DATA ANALYSIS AND RESULTS

The absolute ER cross section is given by

$$\sigma_{ER} = \frac{Y_{ER}}{Y_{MON}} \left[\frac{d\sigma}{d\Omega} \right]_R \frac{1}{\eta_{HYRA}} \Omega_M, \quad (1)$$

where σ_{ER} is the ER cross section, Y_{ER} is the ER yield at the focal plane detector, Y_{MON} is the yield of the elastically scattered particles in the monitor detector, η_{HYRA} is the HYRA transmission efficiency, $[\frac{d\sigma}{d\Omega}]_R$ is the Rutherford differential scattering cross section, and Ω_M is the solid angle subtended by each of the monitor detectors. The differential Rutherford scattering cross section in the laboratory frame is calculated from the formula

$$\frac{d\sigma}{d\Omega} = 1.296 \left[\frac{Z_p Z_t}{E_{lab}} \right]^2 \left[\frac{1}{\sin^4 \left(\frac{\theta}{2} \right)} - 2 \left(\frac{A_P}{A_t} \right)^2 + \cdots \right], \quad (2)$$

where Z_p, Z_t and A_p, A_t are the atomic and mass numbers of the projectile and target, respectively. E_{lab} and θ are,
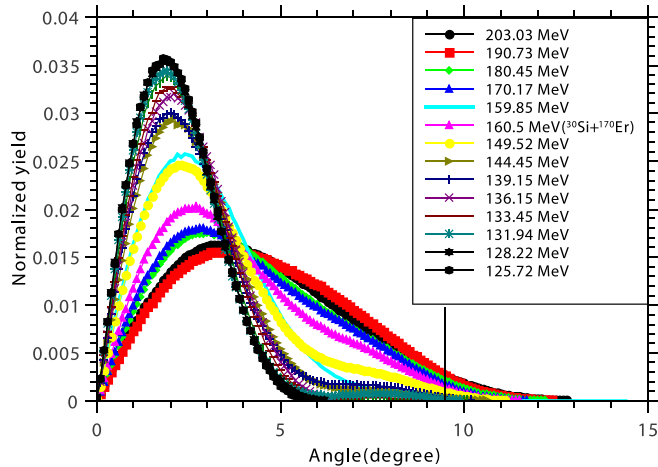
FIG. 1. Normalized angular distributions of ERs simulated using the TERS code. The angular acceptance of HYRA is 9.5° and is also marked in the figure by a vertical line.
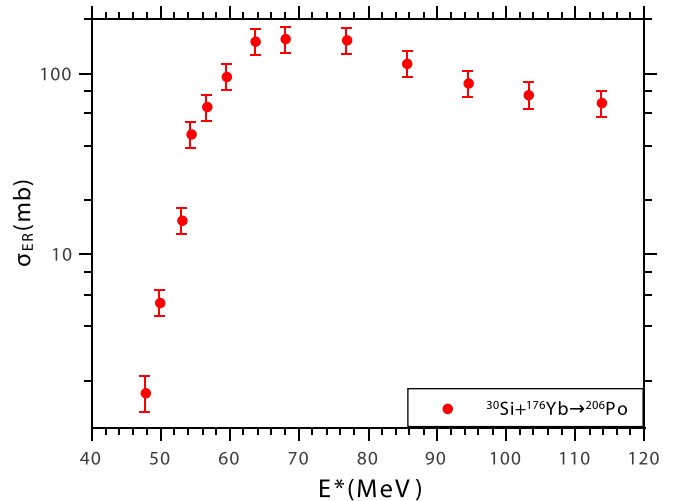

FIG. 2. The experimental ER cross sections for the reaction ^{30}Si + ^{176}Yb as a function of excitation energy.

respectively, the energy of the incident projectile and scattering angle in the laboratory frame.

The transmission efficiency of HYRA is the ratio of the number of ERs detected at the focal plane to the total number of ERs produced at the target chamber. It depends on various parameters such as the entrance-channel mass asymmetry, the beam energy, the target thickness, the exit channel of interest, the angular acceptance of HYRA, the magnetic field and gas pressure settings of HYRA, and the size of the focal plane detector [33,37–39]. In order to calculate the transmission efficiency, the different possible ER channels and their relative yields in the reaction ^{30}Si + ^{176}Yb are obtained using the statistical model code PACE4 [40]. The ER angular distributions for all channels (which contribute more than 1% of total ER cross section) is simulated using the Monte Carlo simulation code TERS [41] at each energy point. This semimicroscopic code takes the actual input parameters during the experiment such as the neutron, proton, and α separation energies, etc. The interaction of the beam with the target is calculated event by event and it generates the reaction distribution of ERs such as angle, energy, and charge state in the output. Here, due to focusing effects, the energy and charge state are assumed to be nearly 100%, but practically the polar acceptance angle of HYRA is 9.5°. The normalized angular distributions at each energy are obtained by adding the individual ER angular distributions with the proper weighted yield. The normalized angular distributions obtained are shown in Fig. 1.

In the present set of measurements, the system ^{30}Si + ^{170}Er is used as the calibration reaction whose ER cross sections are already reported [28]. A measurement of this reaction under the same conditions of HYRA has been carried out at an incident beam energy of 160.5 MeV and has been compared with the previously reported cross sections to obtain the efficiency. From Fig. 1 a multiplication factor is obtained by taking the ratio of area under the angular distribution curves up to 9.5° for ^{30}Si + ^{176}Yb and ^{30}Si + ^{170}Er reactions. This multiplication factor is used to scale the η_{HYRA} obtained for ^{30}Si + ^{170}Er to extract the transmission efficiency for ^{30}Si + ^{176}Yb. The

transmission efficiency extracted for the system ^{30}Si + ^{176}Yb in this manner is 4.5% ± 0.6%.

The total ER cross section obtained for the reaction ^{30}Si + ^{176}Yb as a function of excitation energy is shown in Fig. 2. The measured ER excitation function shows a decreasing trend at higher beam energies. Here, the increased contribution from fission limiting the population of higher ℓ waves, dominates over particle evaporation. The detailed theoretical analysis is included in the following sections.

IV. THEORETICAL ANALYSIS

The ER formation can be considered as a three stage process: 1) capture, 2) fusion, and 3) decay through the energetically possible modes. Hence, in order to calculate the Evaporation residue cross section the first step is the calculation of the capture cross section.

In the present study, in order to calculate the capture cross section, coupled-channels calculations have been carried out using the code CCFULL. The Woods-Saxon parametrization of the Akyz-Winther [42] potential has been used in CCFULL with parameters: the depth V_0, the radius r_0, and the diffuseness parameter a_0. Proper rotational and vibrational couplings to the target and the projectile have been taken into account. The potential parameters (V_0, r_0, and a_0) are taken as −73.94 MeV, 1.179 fm, and 0.676 fm, respectively. Rotational levels up to five states of ^{176}Yb are accounted for in the calculations. The effects of quadrupole ($\beta_2 = 0.289$) and hexadecapole ($\beta_4 = -0.068$) deformations of the ^{176}Yb nucleus are also accounted for. The deformation parameters used in CCFULL are taken from the standard tables [43,44].

The statistical model [45] calculations have been used to analyze the ER cross sections in the above barrier region. The emission of light particles (n, p, α), γ rays, and fission are the main decay mechanisms of the complex nucleus in these computations. The Weisskopf formula [46] is used to calculate the decay width of light particles and γ rays. The fission decay width and nuclear level density are important parameters in

the statistical model. The Kramers' fission decay width is employed in the current calculations [47] and is given by

$$K_{\text{Kramers}} = \frac{\hbar \omega_{\text{g.s.}}}{T \omega_{sp}} \left[\sqrt{\omega_{sp}^2 + \frac{\eta^2}{4}} - \left(\frac{\eta}{2} \right) \right]. \qquad (3)$$

η is the dissipation coefficient, ω_{gs} and ω_{sp} are the curvatures of the potential at the ground state and saddle point, respectively. The Fermi gas model is used to calculate the temperature T. The excitation energy (U) dependent level-density parameter a, by incorporating the shell effects, as per the prescriptions of Ignatyuk is utilized and is given as [48]

$$a = \tilde{a} \left[1 + \frac{F(U)}{U} \delta U \right], \qquad (4)$$

where

$$F(U) = 1 - \exp(-\gamma U) \qquad (5)$$

and

$$\tilde{a} = \alpha A + \beta A^{2/3} B_s, \qquad (6)$$

where δU is the shell correction, which is the difference between the experimental binding energy of a nucleus and the binding energy calculated using the liquid drop model and α, β, and the damping factor, γ are the coefficients in the level density calculations [49]. The dimensionless quantity $B_s(\beta_2)$ is the ratio of the surface area of the deformed nucleus, with the quadrupole deformation parameter β_2, to the area of the spherical nucleus having equal volume. The quantity $B_s(\beta_2)$ is calculated for the deformation of the ground state (widths of particle emission) and for the saddle point (fission width). The values of the deformation of the nucleus at the saddle point are calculated according to Ref. [50]. The ground-state properties of nuclei (mass, shell correction, and deformation) are taken from [44]. The ground-state masses for known nuclei are taken from [51]. The fission barrier is calculated using the formula

$$B_{\text{fiss}}(U) = B_{\text{LDM}} - \delta U, \qquad (7)$$

where B_{LDM} is the liquid-drop fission barrier [52].

The survival probability was calculated using the Monte Carlo method. At each step of decay of the excited nucleus, one of the various outcomes, such as neutron, proton, α-particle or γ-ray emission, or fission, is chosen at random. Ground state masses for known nuclei are taken from [51]. The relevant probability of each event is

$$P = \frac{\Gamma_x}{\Gamma_{\text{Tot}}}, x = n, p, \alpha, \gamma, \text{fission}. \qquad (8)$$

$$\Gamma_{\text{Tot}} = \Gamma_n + \Gamma_p + \Gamma_\alpha + \Gamma_\gamma + \Gamma_{\text{fission}}. \qquad (9)$$

According to the statistical model approach, when a statistical equilibrium is reached, all open channels are likely to be populated. After capture, the system forms the CN and then de-excites by all energetically possible decay modes like particle evaporation, γ decay, and fission.

In the present case, statistical model calculations have been performed to analyze the experimentally measured ER cross sections. The capture cross sections calculated using CCFULL
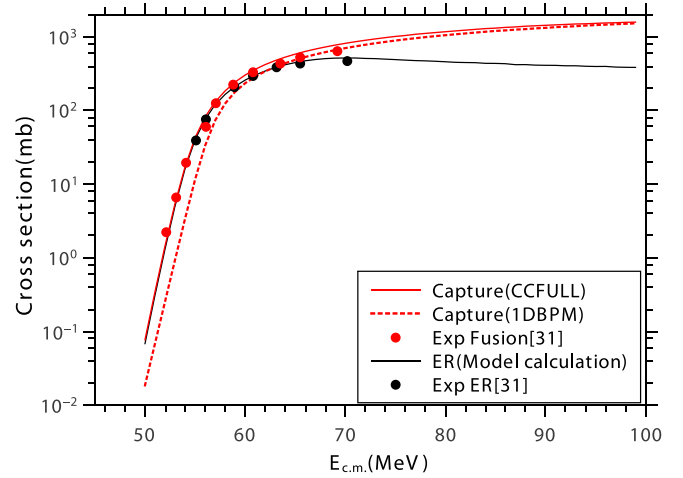

FIG. 3. The experimental ER cross sections for the reaction ^{12}C + ^{194}Pt compared with those from the statistical model calculation. The capture cross sections predicted by CCFULL and 1DBPM are also shown.

have been used as the input to the statistical model calculations. In order to optimize, the parameters similar calculations are performed for another system, with larger asymmetry, namely, ^{12}C + ^{194}Pt, producing the same compound nucleus. The potential parameters are optimized by matching the experimental fusion cross sections with those obtained using the CCFULL calculations [31]. To compare the experimental ER cross sections with the theoretical predictions for the ^{12}C + ^{194}Pt system the statistical model code is used with the dissipation coefficient η in the Kramers' fission width and the damping factor γ in the level density as adjustable parameters. Both total fusion cross sections and ER cross sections are specifically reported using the assumption of true compound nucleus formation. Statistical model calculations reproduce the experimental ER cross sections for the system ^{12}C + ^{194}Pt perfectly as shown in Fig. 3. Similar model calculations are also performed for the ^{30}Si + ^{176}Yb reaction using similar values for the parameters η and γ as used for the ^{12}C + ^{194}Pt system and it is shown in Fig. 4. From Fig. 4 it is clear that there is a remarkable shift in the measured ER cross sections and the cross sections calculated using statistical models at higher incident energies.

V. DISCUSSION

ER production is the clearest indication of compound nucleus formation. The comparison of the ER cross sections for the two systems, forming the same compound nucleus, at the same excitation energy, will provide an insight to the involvement of noncompound nuclear reaction mechanisms such as quasifission. In order to see the extent of the discrepancy in the measured and calculated ER cross sections, in other words the contribution of quasifission in these cases, the reduced ER cross sections (Σ_{ER}) for ^{12}C + ^{194}Pt and ^{30}Si + ^{176}Yb systems, are plotted in Fig. 5. To deduce the reduced cross sections for the systems, the fusion function method [53] is used. This method adopts the transformations for energy and cross
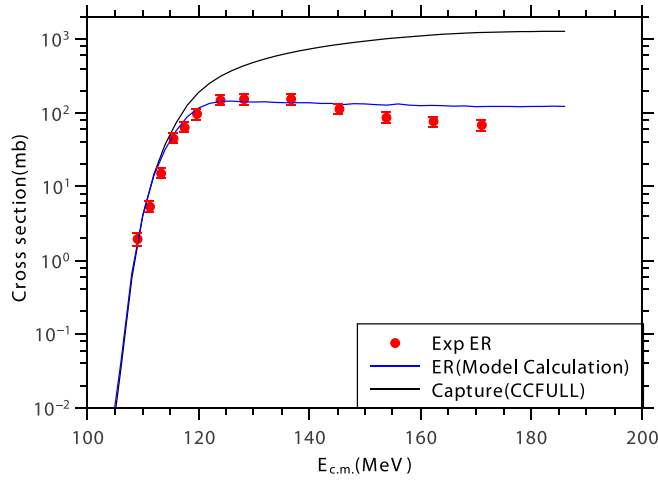
FIG. 4. The experimental ER cross sections for the reaction ^{30}Si + ^{176}Yb compared with those of the statistical model calculation.

section as, $E \rightarrow \epsilon$ and $\sigma_{ER} \rightarrow \Sigma_{ER}$:

$$\epsilon = \frac{E - V_B}{\hbar\omega} \qquad (10)$$

and

$$\Sigma_{ER} = \sigma\left[\frac{2E}{\hbar\omega R_B^2}\right]. \qquad (11)$$

In this method, the potential barrier is fitted with a parabola with V_B, the barrier height located at R_B, and curvature parameter $\hbar\omega$, where R_B is the fusion radius. Fusion radius, R_B is obtained from the CCFULL calculations. From Fig. 5, it can be seen that the reduced cross sections for the presently studied system, ^{30}Si + ^{176}Yb, are significantly lesser when compared with those of ^{12}C + ^{194}Pt, which is much more asymmetric than the present system. The theoretical calculations reproduce the reduced cross section for the asymmetric system satisfactorily over the reported range. According to Bohr's
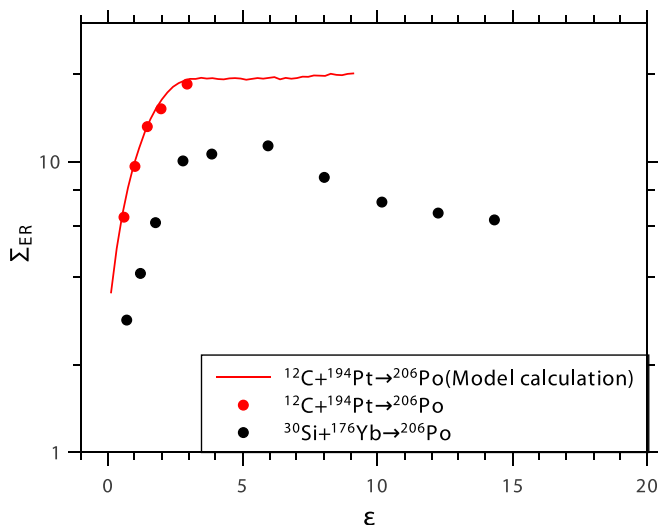

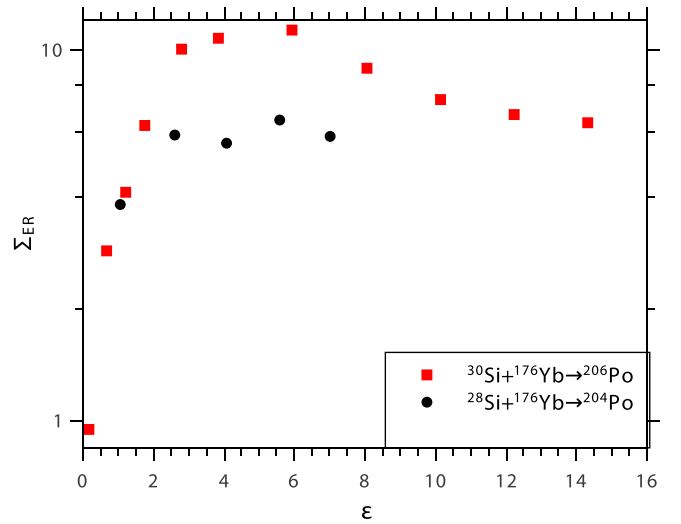FIG. 5. The reduced ER cross sections for the systems ^{12}C + ^{194}Pt and ^{30}Si + ^{176}Yb.

FIG. 6. The reduced ER cross section for the systems ^{30}Si + ^{176}Yb and ^{28}Si + ^{176}Yb.

hypothesis, once a compound nucleus is formed its decay is independent of its past history. Hence the reduction in the ER cross sections of the ^{30}Si + ^{176}Yb reaction from the statistical model calculations can be adduced to the presence of noncompound nuclear process. In order to have a comparative analysis, the reduced ER cross sections reported by Sudarshan *et al.* [25], for a neighboring compound nucleus, ^{204}Po* produced by the ^{28}Si + ^{176}Yb reaction, along with the present measurement are plotted in Fig. 6. The authors have also measured the average γ ray multiplicities of the ERs produced and concluded that ℓ waves populated close to the entrance channel Coulomb barrier are not large enough to cause a substantial reduction in the fission barrier. This high fission barrier reduces the chance for the complete fusion fission and hence the increased fission contribution can be from the noncompound effect. These two systems have almost the same mass asymmetry with a difference of just two neutrons. In Fig. 6 it is interesting to note that both the measurements show similar trends with a discrepancy in the calculated values of reduced ER cross sections in the high energy region.

The observed reduction in the reduced ER cross sections is an indication of fusion suppression for the more symmetric system. This result is consistent with the fact that mass asymmetry dependence of the potential energy surface can influence the fusion probability [3,6]. The mass asymmetry can be defined as

$$\alpha = \frac{A_T - A_P}{A_T + A_P}, \qquad (12)$$

where A_T and A_P are the target and projectile masses, respectively. For the ^{12}C + ^{194}Pt reaction, $\alpha = 0.883$, which is greater than α_{BG}, the Businaro-Gallone mass asymmetry [54] ($\alpha_{BG} = 0.846$). Hence the driving force due to the nuclear potential favors a compact CN with high survival probability [7]. However, for mass symmetric reactions, for which $\alpha = 0.706$, which is less than α_{BG}, the system breaks without forming a completely equilibrated CN. The comparison also shows the clear dependence of quasifission on the entrance

channel charge product ($Z_p Z_t$). Earlier dynamical models [4,5,55] predicted the onset of quasifission for very heavy systems with the Coulomb factor $Z_p Z_t > 1600$, where Z_p and Z_t are the atomic numbers of the projectile and target, respectively. However, quasifission was reported in many asymmetric reactions using deformed targets at sub- and near-Coulomb barrier energies, even though the $Z_p Z_t$ values were much lower than 1600 [17–19]. The fusion hindrance can also be observed in terms of the static deformation of the target nucleus and also the orientation of the colliding nuclei [9,10]. The static deformation ($\beta_2 = 0.289$) is more for ^{176}Yb than ^{194}Pt ($\beta_2 = 0.13$) and hence the elongated configuration favors the noncompound process.

In Fig. 6, the measured ER cross sections for ^{30}Si are compared with the cross section for the ^{28}Si + ^{176}Yb, reaction. The difference in the measured cross sections could be due to the reduced compound nuclear fissility of ^{206}Po* nuclei with an increase in neutron number. The neutron binding energy decreases with an increase in neutron number, which also favors neutron evaporation in the heavier CN compared to ^{204}Po*. The presence of quasifission can also be explained in terms of isospin asymmetry ($\Delta \frac{N}{Z}$) in the entrance channel. Studying mass angle distributions for different systems Simenel *et al.* [11] have reported the increased contribution of quasifission for systems with large entrance channel isospin asymmetry. In the present case too the increased contribution to the measured cross section could be due to the lower isospin asymmetry in the entrance channel for the ^{30}Si + ^{176}Yb reaction.

The ER cross section can be generally represented as

$$\sigma_{ER}(E_{c.m.}) = \sigma_{capture} P_{CN} P_{survival}(E_{c.m.}), \quad (13)$$

where $\sigma_{capture}$ is the capture cross section for the formation of the dinucleus system and $E_{c.m.}$ is the total entrance channel kinetic energy in the center of mass frame or the available initial energy in the center of mass frame. P_{CN} is the probability of the complete fusion of the dinuclear system to form the compound nuceus, $P_{survival}$ is the fission survival probability of the CN to form ER at a given energy. The probability of true compound nucleus formation is represented by $P_{CN} P_{survival}$. In order to see the effect of the entrance channel and the excitation energy, $P_{CN} P_{survival}$ is calculated for the present analyzed systems as a function of reduced energy and is plotted in Fig. 7. The ER formation probability is calculated using the equation

$$P_{CN} P_{survival} = \frac{\sigma_{ER}}{\sigma_{capture}}. \quad (14)$$

As can be seen from Fig. 7, ER formation probability decreases considerably with decreasing mass asymmetry of the system. Further, the ER formation probability is found to decrease with the excitation energy. It is also noted that a
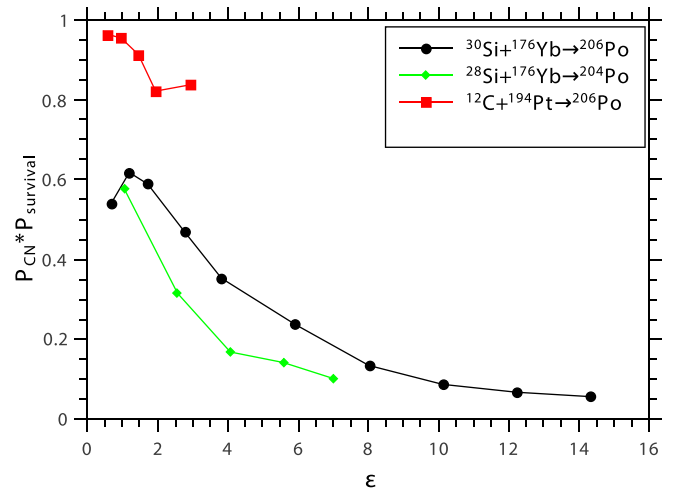

FIG. 7. The ER formation probabilities for the systems ^{30}Si + ^{176}Yb, ^{28}Si + ^{176}Yb, and ^{12C}C + ^{194}Pt.

significant effect of isospin asymmetry has also been observed in the reference system.

VI. SUMMARY AND CONCLUSIONS

ER cross sections have been measured for the system ^{30}Si + ^{176}Yb forming the compound nucleus ^{206}Po*. A comparison of the ER cross sections for two reactions populating the same CN with the statistical model calculations, for the same set of parameters, shows a reduction in ER cross sections for more symmetric reactions with larger $Z_P Z_T$ and increased deformation of the target. This reduction is a direct signature of fusion hindrance due to noncompound nuclear process in heavier systems and its dependence on entrance channels. Another comparison with a similar system, forming a neighboring nucleus as the compound nucleus, shows that the ER cross sections are larger for the system with larger neutron number. As the compound nucleus' neutron number increases, the neutron binding energy and compound nuclear fissility decreases and hence the compound nucleus with larger neutron number becomes more stable against fission.

ACKNOWLEDGMENTS

[1] J. D. Bierman, P. Chan, J. F. Liang, M. P. Kelly, A. A. Sonzogni, and R. Vandenbosch, Phys. Rev. Lett. **76**, 1587 (1996).

[2] K. Hagino, N. Takigawa, M. Dasgupta, D. J. Hinde, and J. R. Leigh, Phys. Rev. Lett. **79**, 2014 (1997).

[3] A. C. Berriman, D. J. Hinde, M. Dasgupta, C. R. Morton, R. D. Butt, and J. O. Newton, Nature (London) **413**, 144 (2001).

[4] D. Hinde and M. Dasgupta, Phys. Lett. B **622**, 23 (2005).

[5] K. Nishio, S. Mitsuoka, I. Nishinaka, H. Makii, Y. Wakabayashi, H. Ikezoe, K. Hirose, T. Ohtsuki, Y. Aritomo, and S. Hofmann, Phys. Rev. C **86**, 034608 (2012).

[6] D. J. Hinde, R. du Rietz, M. Dasgupta, R. G. Thomas, and L. R. Gasques, Phys. Rev. Lett. **101**, 092701 (2008).

[7] D. J. Hinde, R. G. Thomas, R. du Rietz, A. Diaz-Torres, M. Dasgupta, M. L. Brown, M. Evers, L. R. Gasques, R. Rafiei, and M. D. Rodriguez, Phys. Rev. Lett. **100**, 202701 (2008).

[8] D. J. Hinde, M. Dasgupta, J. R. Leigh, J. C. Mein, C. R. Morton, J. O. Newton, and H. Timmers, Phys. Rev. C **53**, 1290 (1996).

[9] D. J. Hinde, M. Dasgupta, J. R. Leigh, J. P. Lestone, J. C. Mein, C. R. Morton, J. O. Newton, and H. Timmers, Phys. Rev. Lett. **74**, 1295 (1995).

[10] G. N. Knyazheva, E. M. Kozulin, R. N. Sagaidak, A. Y. Chizhov, M. G. Itkis, N. A. Kondratiev, V. M. Voskressensky, A. M. Stefanini, B. R. Behera, L. Corradi, E. Fioretto, A. Gadea, A. Latina, S. Szilner, M. Trotta, S. Beghini, G. Montagnoli, F. Scarlassara, F. Haas, N. Rowley *et al.*, Phys. Rev. C **75**, 064602 (2007).

[11] C. Simenel, D. Hinde, R. du Rietz, M. Dasgupta, M. Evers, C. Lin, D. Luong, and A. Wakhle, Phys. Lett. B **710**, 607 (2012).

[12] A. Wakhle, C. Simenel, D. J. Hinde, M. Dasgupta, M. Evers, D. H. Luong, R. du Rietz, and E. Williams, Phys. Rev. Lett. **113**, 182502 (2014).

[13] D. J. Hinde, M. Dasgupta, and A. Mukherjee, Phys. Rev. Lett. **89**, 282701 (2002).

[14] V. S. Ramamurthy, S. S. Kapoor, R. K. Choudhury, A. Saxena, D. M. Nadkarni, A. K. Mohanty, B. K. Nayak, S. V. Sastry, S. Kailas, A. Chatterjee, P. Singh, and A. Navin, Phys. Rev. Lett. **65**, 25 (1990).

[15] J. C. Mein, D. J. Hinde, M. Dasgupta, J. R. Leigh, J. O. Newton, and H. Timmers, Phys. Rev. C **55**, R995(R) (1997).

[16] J. P. Lestone, A. A. Sonzogni, M. P. Kelly, and R. Vandenbosch, J. Phys. G: Nucl. Part. Phys. **23**, 1349 (1997).

[17] R. Rafiei, R. G. Thomas, D. J. Hinde, M. Dasgupta, C. R. Morton, L. R. Gasques, M. L. Brown, and M. D. Rodriguez, Phys. Rev. C **77**, 024606 (2008).

[18] R. G. Thomas, D. J. Hinde, D. Duniec, F. Zenke, M. Dasgupta, M. L. Brown, M. Evers, L. R. Gasques, M. D. Rodriguez, and A. Diaz-Torres, Phys. Rev. C **77**, 034610 (2008).

[19] C. Yadav, R. G. Thomas, R. K. Choudhury, P. Sugathan, A. Jhingan, S. Appannababu, K. S. Golda, D. Singh, I. Mukul, J. Gehlot, E. Prasad, and H. J. Wollersheim, Phys. Rev. C **86**, 034606 (2012).

[20] R. Tripathi, K. Sudarshan, S. Sodaye, A. V. R. Reddy, K. Mahata, and A. Goswami, Phys. Rev. C **71**, 044616 (2005).

[21] R. Tripathi, K. Sudarshan, S. Sodaye, A. Goswami, A. V. R. Reddy, and K. Mahata, Int. J. Mod. Phys. E **17**, 419 (2008).

[22] R. Vandenbosch and J. R. Huizenga, *Nuclear Fission* (Academic, London, 1973).

[23] I. Halpern and V. M. Strutinsky, in *Proceedings of the Second United Nations International Conference on Peaceful Uses of Atomic Energy, Geneva, 1958*, edited by J. H. Martens *et al.* (United Nations, Switzerland, 1958), Vol. 15, p. 408.

[24] R. Tripathi, K. Sudarshan, S. K. Sharma, K. Ramachandran, A. V. R. Reddy, P. K. Pujari, and A. Goswami, Phys. Rev. C **79**, 064607 (2009).

[25] K. Sudarshan, R. Tripathi, S. Sodaye, S. K. Sharma, P. K. Pujari, J. Gehlot, N. Madhavan, S. Nath, G. Mohanto, I. Mukul, A. Jhingan, and I. Mazumdar, Phys. Rev. C **95**, 024604 (2017).

[26] A. Shamlath, E. Prasad, N. Madhavan, P. V. Laveen, J. Gehlot, A. K. Nasirov, G. Giardina, G. Mandaglio, S. Nath, T. Banerjee, A. M. Vinodkumar, M. Shareef, A. Jhingan, T. Varughese, D. Kumar, P. S. Devi, Khushboo, P. Jisha, N. Kumar, M. M. Hosamani *et al.*, Phys. Rev. C **95**, 034610 (2017).

[27] A. Shamlath, M. Shareef, E. Prasad, P. Sugathan, R. Thomas, A. Jhingan, S. Appannababu, A. Nasirov, A. Vinodkumar, K. Varier, C. Yadav, B. Babu, S. Nath, G. Mohanto, I. Mukul, D. Singh, and S. Kailas, Nucl. Phys. A **945**, 67 (2016).

[28] G. Mohanto, N. Madhavan, S. Nath, J. Sadhukhan, J. Gehlot, I. Mazumdar, M. Naik, E. Prasad, I. Mukul, T. Varughese, A. Jhingan, R. Bhowmik, A. Sinha, D. Gothe, P. Chavan, S. Pal, V. Ramamurthy, and A. Roy, Nucl. Phys. A **890–891**, 62 (2012).

[29] D. J. Hinde, J. R. Leigh, J. O. Newton, W. Galster, and S. Sie, Nucl. Phys. A **385**, 1 (1982).

[30] K. K. Rajesh, M. M. Musthafa, N. Madhavan, S. Nath, J. Gehlot, J. Sadhukhan, P. M. Aslam, P. T. M. Shan, E. Prasad, M. M. Hosamani, T. Varughese, A. Yadav, V. R. Sharma, V. Srivastava, M. M. Shaikh, M. Shareef, A. Shamlath, and P. V. Laveen, Phys. Rev. C **100**, 044611 (2019).

[31] A. Shrivastava, S. Kailas, A. Chatterjee, A. M. Samant, A. Navin, P. Singh, and B. S. Tomar, Phys. Rev. Lett. **82**, 699 (1999).

[32] N. Madhavan, S. Nath, A. K. Sinha, S. Kalkal, K. M. Varier, M. C. Radhakrishna, J. Das, and R. Singh, Pramana - J. Phys. **75**, 317 (2010).

[33] E. Prasad, K. M. Varier, N. Madhavan, S. Nath, J. Gehlot, S. Kalkal, J. Sadhukhan, G. Mohanto, P. Sugathan, A. Jhingan, B. R. S. Babu, T. Varughese, K. S. Golda, B. P. Ajith Kumar, B. Satheesh, S. Pal, R. Singh, A. K. Sinha, and S. Kailas, Phys. Rev. C **84**, 064606 (2011).

[34] S.Nath, a Monte Carlo code to model ion transport in dilute gas medium (unpublished).

[35] A. Jhingan, Pramana **85**, 483 (2015).

[36] E. T. Subramanium, B. P. Ajith Kumar, and R. K. Bhowmik, http://www.iuac.res.in/NIAS.

[37] G. Mohanto, N. Madhavan, S. Nath, J. Gehlot, I. Mukul, A. Jhingan, T. Varughese, A. Roy, R. K. Bhowmik, I. Mazumdar, D. A. Gothe, P. B. Chavan, J. Sadhukhan, S. Pal, M. Kaur, V. Singh, A. K. Sinha, and V. S. Ramamurthy, Phys. Rev. C **88**, 034606 (2013).

[38] V. Singh, B. R. Behera, M. Kaur, A. Kumar, K. P. Singh, N. Madhavan, S. Nath, J. Gehlot, G. Mohanto, A. Jhingan, I. Mukul, T. Varughese, J. Sadhukhan, S. Pal, S. Goyal, A. Saxena, S. Santra, and S. Kailas, Phys. Rev. C **89**, 024609 (2014).

[39] R. Sandal, B. R. Behera, V. Singh, M. Kaur, A. Kumar, G. Kaur, P. Sharma, N. Madhavan, S. Nath, J. Gehlot, A. Jhingan, K. S. Golda, H. Singh, S. Mandal, S. Verma, E. Prasad, K. M. Varier, A. M. Vinodkumar, A. Saxena, J. Sadhukhan *et al.*, Phys. Rev. C **91**, 044621 (2015).

[40] http://lise.nscl.msu.edu/pace4.

[41] S. Nath, Comput. Phys. Commun. **180**, 2392 (2009).

[42] R. A. Broglia and A. Winther, *Heavy Ion Reaction Lecture Notes*, Elastic and Inelastic Reactions (Benjamin-Cummings, Reading, MA, 1981), Vol. 1.

[43] R. Spear, At. Data Nucl. Data Tables **42**, 55 (1989).

[44] P. Moller, A. Sierk, T. Ichikawa, and H. Sagawa, At. Data Nucl. Data Tables **109–110**, 1 (2016).

[45] https://nrv.jinr.ru.

[46] V. Weisskopf, Phys. Rev. **52**, 295 (1937).

[47] H. Kramers, Physica **7**, 284 (1940).

[48] A. V. Ignatyuk, IAEA Report No. INDC(CCP)-233/L, 1983.

[49] A. Ignatyuk, G. N. Smirenkine, A. S. Tishint, and Y. Fiz, Sov. J. Nucl. Phys. **21**, 612 (1975).

[50] S. Cohen, F. Plasil, and W. Swiatecki, Ann. Phys. (NY) **82**, 557 (1974).

[51] M. Wang, G. Audi, A. Wapstra, F. Kondev, M. MacCormick, X. Xu, and B. Pfeiffer, Chin. Phys. C **36**, 1603 (2012).

[52] A. J. Sierk, Phys. Rev. C **33**, 2039 (1986).

[53] L. F. Canto, D. R. Mendes Junior, P. R. S. Gomes, and J. Lubian, Phys. Rev. C **92**, 014626 (2015).

[54] U. L. Businaro and S. Gallone, Il Nuovo Cimento **5**, 315 (1957).

[55] R. Schmitt, L. Cooke, H. Dejbakhsh, D. Haenni, T. Shutt, B. Srivastava, and H. Utsunomiya, Nucl. Phys. A **592**, 130 (1995).